2015-01-0252
Published 04/14/2015

doi:10.4271/2015-01-0252
saealtpow.saejournals.org

Model-Based Parameter Identification of Healthy and Aged Li-ion Batteries for Electric Vehicle Applications

Ryan Ahmed
McMaster Univ.

Javier Gazzarri
MathWorks Inc.

Simona Onori
Clemson Univ.

Saeid Habibi
McMaster Univ.

Robyn Jackey and Kevin Rzemien
MathWorks Inc.

Jimi Tjong
Ford Motor Co.

Jonathan LeSage
MathWorks Inc.

ABSTRACT

Electric vehicles are receiving considerable attention because they offer a more efficient and sustainable transportation alternative compared to conventional fossil-fuel powered vehicles. Since the battery pack represents the primary energy storage component in an electric vehicle powertrain, it requires accurate monitoring and control. In order to effectively estimate the battery pack critical parameters such as the battery state of charge (SOC), state of health (SOH), and remaining capacity, a high-fidelity battery model is needed as part of a robust SOC estimation strategy. As the battery degrades, model parameters significantly change, and this model needs to account for all operating conditions throughout the battery's lifespan. For effective battery management system design, it is critical that the physical model adapts to parameter changes due to aging.

In this paper, we present an effective method for offline battery model parameter estimation at various battery states of health. An equivalent circuit with one voltage source, one resistance in series, and several RC pairs modeled the battery charging and discharging dynamics throughout the lifespan of the battery. Accelerated aging tests using real-world driving cycles simulated battery usage. Three lithium nickel-manganese-cobalt oxide (LiNiMnCoO2) cells were tested at temperatures between 35°C and 40°C, with interruptions at every 5% capacity degradation to run reference performance tests for tracking changes in the battery model parameters. The equivalent circuit-based model was validated using real-world driving cycles. The parameter estimation procedure resulted in an efficient model that keeps track of the battery evolution as it ages.

CITATION: Ahmed, R., Gazzarri, J., Onori, S., Habibi, S. et al., "Model-Based Parameter Identification of Healthy and Aged Li-ion Batteries for Electric Vehicle Applications," *SAE Int. J. Alt. Power.* 4(2):2015, doi:10.4271/2015-01-0252.

INTRODUCTION

During the last several years, hybrid electric vehicles (HEVs) and battery electric vehicles (BEVs) have received considerable attention due to their efficiency and sustainability []. Batteries, a component of paramount importance for these types of vehicles, require accurate real-time monitoring and control in order to avoid any overcharge or over discharge conditions that shorten their lifespan and impact safety.

The battery management system (BMS) is responsible for monitoring the battery state-of-charge (SOC), state-of-health (SOH), state-of-power (SOP), and remaining useful life [2]. The BMS also performs thermal management, cell balancing, and attempts to avoid battery overcharge or under-discharge that might affect driver safety and shorten battery life. The battery SOC, SOH, and SOP are three key variables used in battery condition monitoring and energy management. Since electric vehicles have been on the market for a relatively short period of time, possible battery malfunction or severe fires would result in loss of market share and in a move away from electric vehicles. Therefore, an adaptive BMS is necessary to account for degradation in performance that might affect vehicle drivability and range of operation.

The performance and safety of HEVs and BEVs are highly dependent on the accurate and immediate assessment of the SOC, which is the amount of charge available for use by the vehicle at any time. The range, fuel economy, and other critical calculated performance criteria rely greatly on the SOC. Consequently, accurately estimating the SOC will ultimately improve both vehicle safety and customer satisfaction. The SOH is often related to the loss of rated capacity. When the capacity reduces to 80% of the beginning of life capacity, the battery is considered to have reached its end of life. Cycling and calendar aging cause the battery to lose its capacity.

Battery models are typically classified as one of the following: equivalent circuit-based models, behavioral models, or electrochemical models. **Equivalent circuit-based models** use basic RC circuit elements such as resistors and capacitors to model battery dynamics. Equivalent circuit-based models are simple, computationally efficient, and can be easily implemented onboard a BMS. **Behavioral models** are empirical and utilize various functions to model battery dynamics. In [3], Plett introduced a series of behavioral models, namely: the combined model, the simple model, the zero-state hysteresis model, the one-state hysteresis model, and the enhanced self-correcting model. These models can be easily optimized and they account for Ohmic losses, hysteresis, and polarization time constants. **Electrochemical models** utilize partial differential equations to model lithium intercalation inside the electrolyte and both electrodes. Since electrochemical models provide a physical insight of the battery chemistry, they are favored in SOH estimation and in tracking battery degradation. However, in general, electrochemical models have numerous parameters that are hard to set, are relatively complex, and require more computational power. Therefore, for their application in real-time BMS, these models need to be simplified and reduced to an appropriate level of dynamic significance [3].

In prior work [4], a battery aging study was conducted using current profiles at fixed C-rates to age the battery, however this did not reflect real-world driving conditions. Electric vehicle batteries are subjected to high transients resulting from vehicle acceleration and regenerative braking. Accordingly, this paper addresses the issue by conducting an aging scenario for a BEV, assuming an average North-American driver. These tests were conducted over a 12-month period and involved accelerated testing of battery lifetime at temperatures between 35 °C and 40 °C using current profiles from real-world driving cycles, such as the Urban Dynamometer Driving Schedule (UDDS). An equivalent circuit with one voltage source, one resistance in series, and several RC pairs was used to model the battery charging and discharging dynamics throughout the anticipated lifespan of the battery. This model provides a good compromise between model accuracy and simplicity for real-time BMS implementation. A parameter estimation method implemented in MATLAB utilized optimization functions to fit simulation results to experimental data. The parameter estimation procedure clearly showed dependencies of the equivalent circuit model parameters on the battery state of charge and state of life. These dependencies were implemented as lookup tables to be used in simulation.

This paper is organized as follows: First, we describe the electric vehicle model development to generate the current profile required for experimentation. Second, we provide a summary of the aging experiments. Third, we describe the experimental setup used for data collection. Fourth, we focus on the battery model and the identification of equivalent circuit model parameters during the cell's lifespan. Fifth, we discuss the experimental results and the cell changes due to aging. Finally, we outline conclusions and applicability of the proposed method.

ELECTRIC VEHICLE MODEL AND CURRENT GENERATION

This section describes the electric vehicle model used to generate the current profile from the velocity profile of various driving cycles. A mid-size BEV model, as shown in Figure 1, was modified from an existing hybrid vehicle model [5]. The model was developed in Simulink using Simscape library components. At a fully charged state, the driving range of the simulated BEV is approximately 200 km. Figure 1 shows the BEV model consisting of a lithium-ion battery pack, a vehicle speed controller, vehicle dynamic model, electric motor, and DC-DC converter.

Three benchmark driving schedules were considered in this study, namely: a UDDS, a light duty drive cycle for high speed and high load (US06), and a highway fuel economy test (HWFET) [5]. The UDDS driving cycle is used to characterize a city driving condition. Its purpose is to replicate average speed, idle time, and number of stops for an average driver.

The US06 cycle is a high acceleration, aggressive driving cycle, and the HWFET embodies highway driving conditions with speeds below 60 miles per hour [6]. The three above mentioned driving cycles are shown in Figure 3. A summary of these driving cycle characteristics such as distance, time, and average speed is provided in Table 1 [6].

The pack current profiles from these driving cycles are shown in Figure 3. The pack-level current profiles have been scaled down to the cell level while ignoring cell-to-cell balancing.

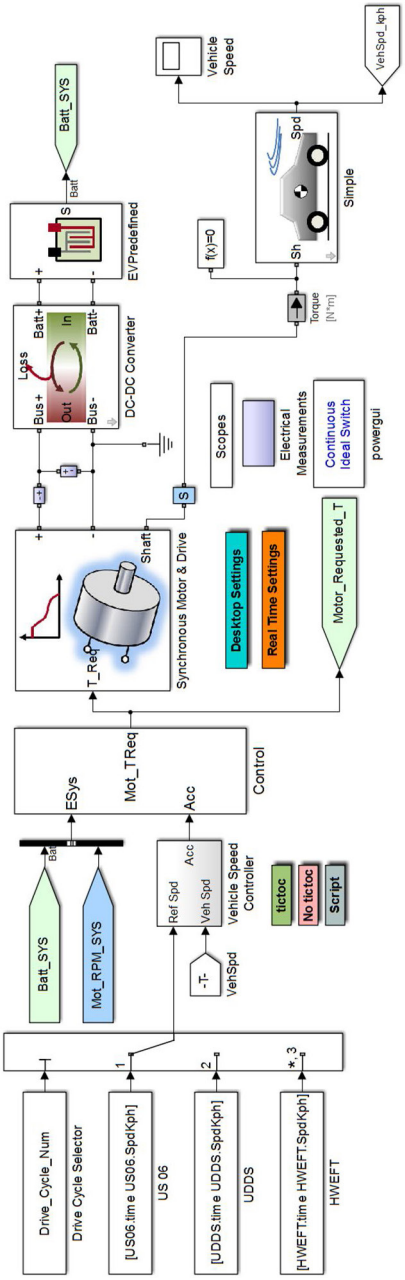

Figure 1. All-electric, mid-size sedan simulation model in Simscape (adopted from [5]).

Table 1. Characteristics of UDDS, US06, and HWFET driving schedules, [6].

	Time (sec)	Distance (km / miles)	Average Speed (kph / mph)
UDDS	1,369	12 / 7.45	31.5 / 19.59
US06	596	12.9 / 8.01	77.8 / 48.37
HWFET	765	16.5 / 10.26	77.7 / 48.30

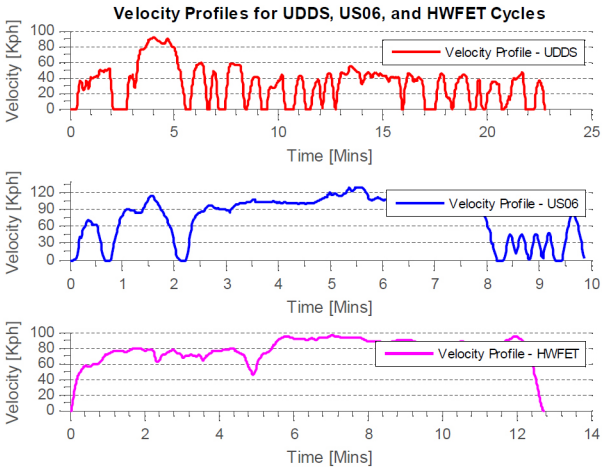

Figure 2. Velocity profiles for the UDDS (upper), US06 (middle), and HWFET (lower) cycles [6]

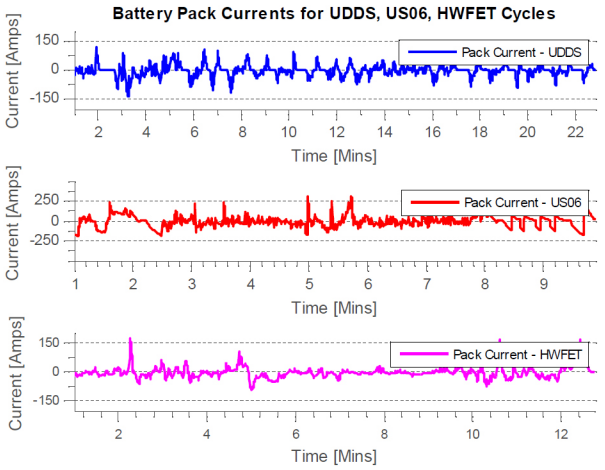

Figure 3. Pack current profiles for the UDDS (upper), US06 (middle), and HWFET (lower) cycles.

AGING STUDY OVERVIEW

Laboratory tests are conducted on battery cells, modules, and packs in order to assess their performance at various states of life and temperature conditions [7]. Data collected during these tests can be used to estimate battery model parameters and validate battery models that are essential for SOC and SOH estimation.

In this paper, two test schedules are considered: Schedule A for Reference Performance Tests (RPTs) and Schedule B for Aging Tests. The RPTs involve a static capacity test at 1C and pulse charge and discharge test. RPTs are conducted every 15 simulated weeks to track degradation in performance as the battery ages. All aging tests were conducted at elevated temperatures (between 35-40°C) to accelerate aging and thus acquire the experimental data in a reduced period of time.

Schedule A - Reference Performance Tests

RPTs capture battery cell baseline performance characteristics such as cell power capability, internal resistance, capacity, and time constants. Tests selected for the study include static capacity and pulse charge and discharge.

Static Capacity Test

The static capacity test measures the battery cell capacity in amperehours at a constant current (CC) discharge rate. This discharge rate, or C-rate, is dictated by the capacity of the battery. For example, a 1Ah battery has a C-rate of 1C when the battery is discharged in one hour, i.e., with a current of 1A. This test provides a baseline for a fresh battery cell capacity. The test procedure follows the constant-current constant-voltage (CCCV) protocol and consists of the following steps [3]:

1. Charge the battery at 1C rate (5.4 A) to the fully charged state in CCCV mode. The battery is fully charged to 4.2 V when the current end point is at 0.02 C (0.108 A).
2. Let the battery rest for one hour in order to allow for voltage and current stabilization.
3. Discharge sequence at a constant current 1C rate until the voltage reaches the battery minimum limit of 2.8 V as recommended by the manufacturer.
4. Let the battery rest with no load for one hour.

Pulse Charge and Discharge Test

The pulse charge and discharge test characterizes the battery voltage response (cell dynamics) at various states of charge and current rates. The test comprises a series of discharge and charge pulses across the full SOC range. The test procedure is summarized as follows:

1. Charge the battery to a fully charged state.
2. Let the battery rest for one hour for voltage and current stabilization [3].
3. Discharge the battery with pulses of 1% of capacity from 100% to 90% SOC at 1C rate and allow for one-hour rest periods between pulses.
4. In the 90% to 10% SOC range, discharge the battery by 5% capacity steps at 1C rate and allow for four hours rest between cycles.
5. In the range between 10% and 0% SOC, discharge the battery by pulses of 1% of capacity at 1C rate while allowing a one-hour rest between cycles.

Schedule B - Aging (Cycle Life) Tests

The purpose of aging tests is to study the process of battery degradation due to multiple charge and discharge cycles [7] mimicking a driver's behavior in real-world driving conditions. The present study combines UDDS, US06, and HWFET driving schedules (Table 2). These tests are defined based on a target velocity profile and its corresponding current profile for an all-electric, midsize sedan vehicle modeled in Simscape.

Schedule B consists of a combination of driving cycles that discharge the battery down to 25% SOC. The test is conducted at elevated temperatures in the range of 35°C - 40°C to accelerate aging. The description of Schedule B for both weekday and weekend is as shown in Figure 4 and Figure 5, respectively [8].

Table 2. Aging Schedule B scenario [8]

Trip	Drive Cycle Combination	Frequency	Description
Work	$UDDS_t$+ $US06_t$+ $UDDS_t$+ $US06_t$	Twice Daily 5 days/week 48 weeks/year	Starting from a fully charged state, a commute from home to work and back with no charge at work
Weekend / Vacation	$UDDS_t$+ $HWFET_t$ + $HWFET_t$+ $HWFET_t$+ $HWFET_t$+ $UDDS_t$+ $UDDS_t$+ $HWFET_t$ + $HWFET_t$+ $HWFET_t$+ $HWFET_t$+ $UDDS_t$	2 days/week 124 days/year	Starting from a fully charged state, assuming no charging station at the weekend destination

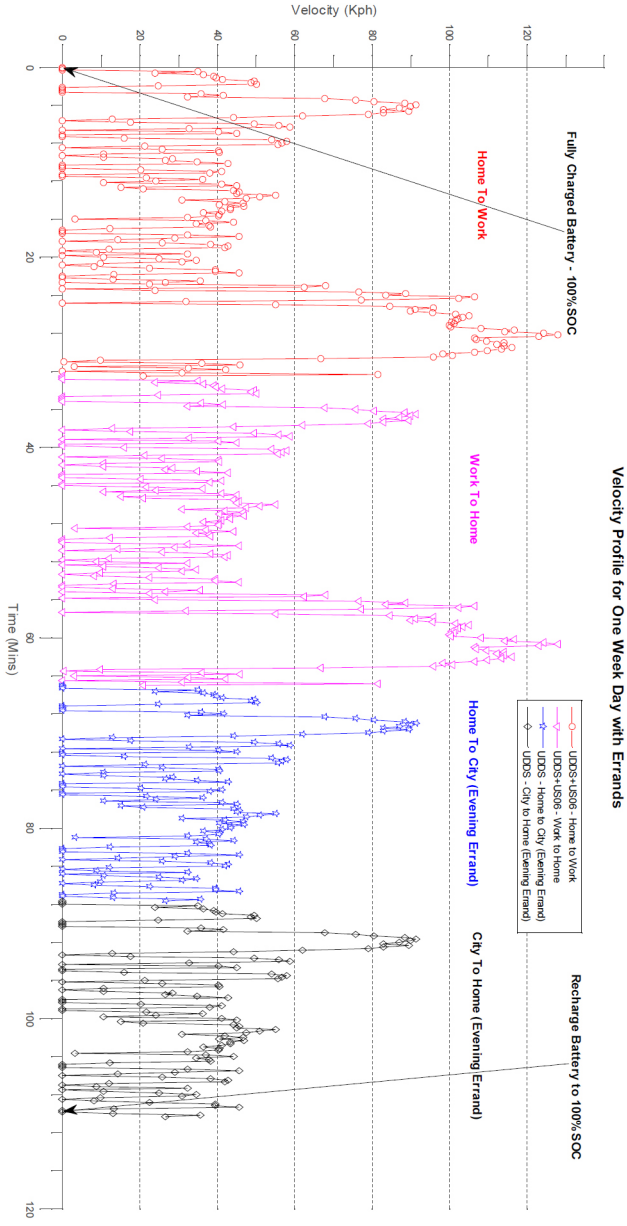

Figure 4. Schedule B: One weekday of driving with errands.

Current profile, voltage, and SOC from one aging week are shown in Figure 6. The SOC varies from 25% to 90% every day. The battery is then fully charged at the end of each day. Current values range from - 2C to 2C and voltages from 3.6V to a maximum of 4.2V. Current, SOC, and Voltage for one weekday of driving are shown in Figure 7, and for one weekend of driving are shown in Figure 8.

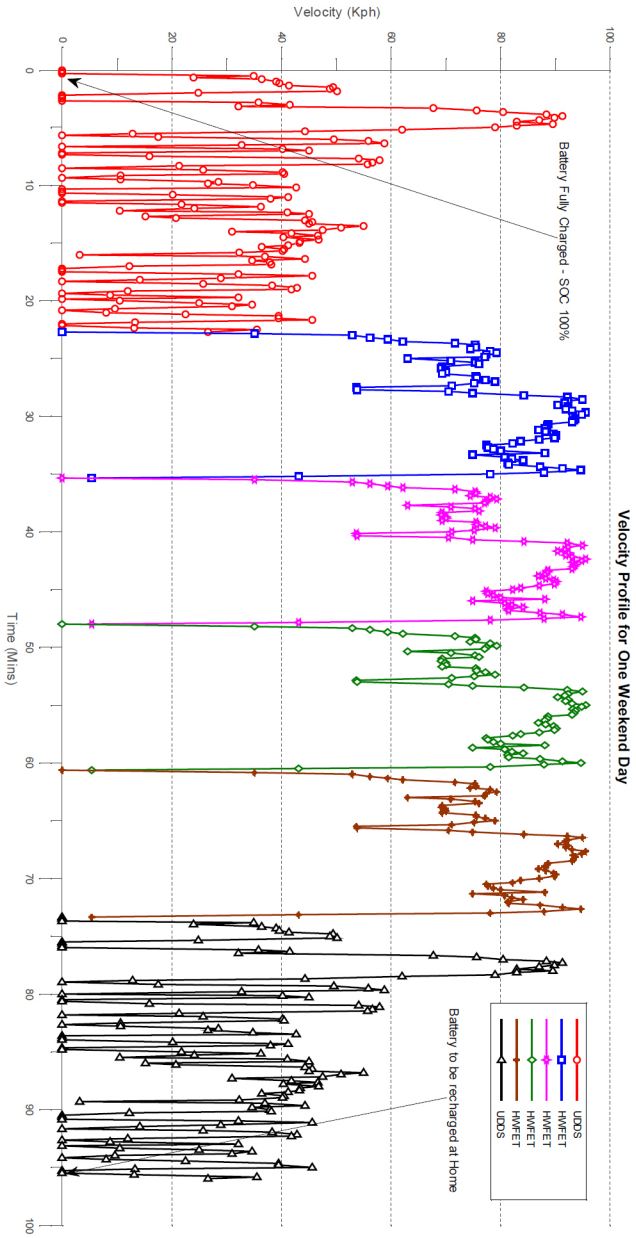

Figure 5. Schedule B: One weekend day driving.

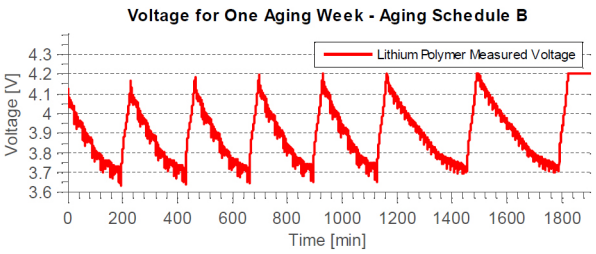

Figure 6.

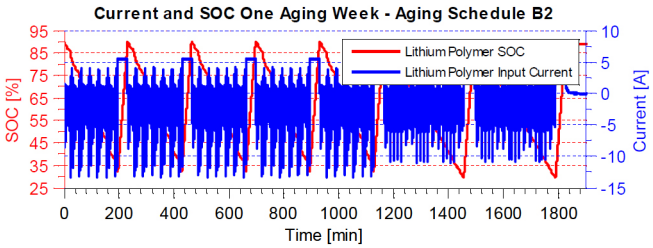

Figure 6. (cont.) Voltage (upper), current, and SOC (lower) for one aging week - Schedule B.

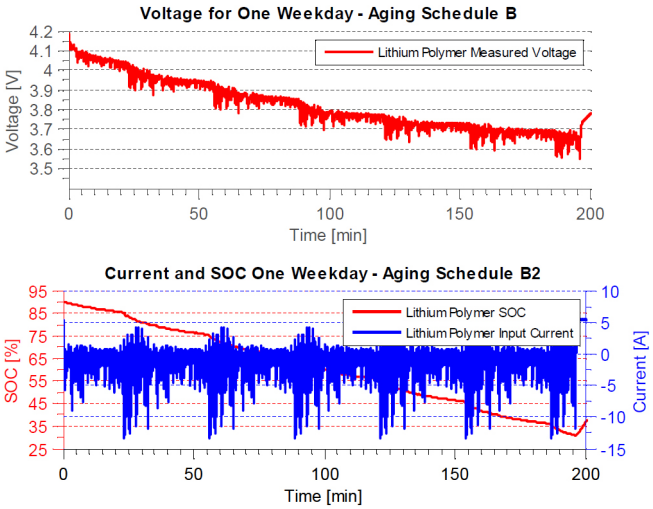

Figure 7. Voltage (upper), current, and SOC (lower) for one weekday - Schedule B.

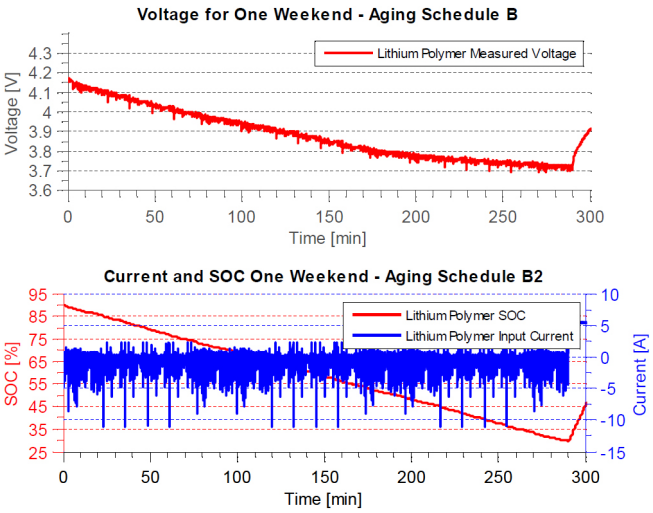

Figure 8. Voltage (upper), current, and SOC (lower) for one weekend - Schedule B.

Experimental Setup

Figure 9, Figure 10, and Figure 11 show the experimental setup utilized for the tests. The setup includes a 3-channel Arbin BT2000 tester, three NMC lithium polymer battery cells, three environmental chambers, an AVL Lynx data acquisition system, and AVL Lynx user interface software. AVL Lynx software is used for setting up the test procedure

and for data acquisition. Variables such as battery current, voltage, and temperatures during charging, discharging, and rest phases are acquired at a maximum frequency of 50 Hz.

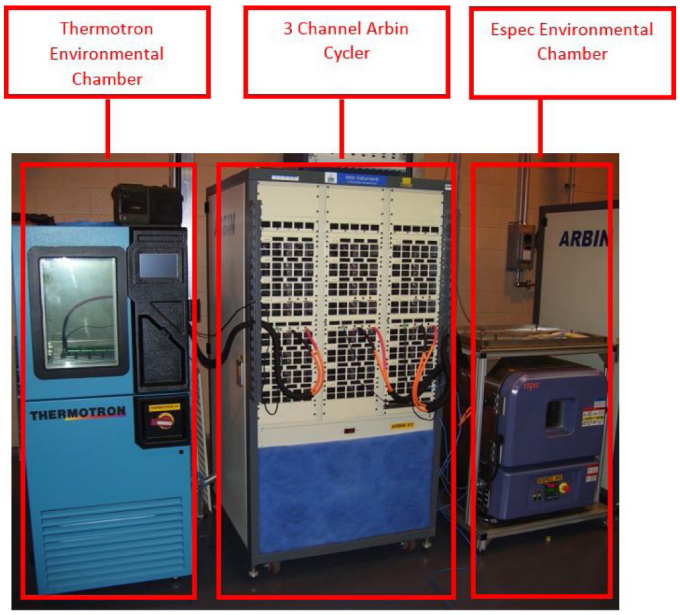

Figure 9. Arbin BT2000 Cycler along with Espec and Thermotron environmental chambers

Figure 10. Experimental setup including cyclers, environmental chambers, and data acquisition systems.

Battery cells are placed in environmental chambers in order to perform the test at controlled temperature.

Each battery was independently tested using a separate tester channel. Figure 11 shows the Arbin tester. The tester has three independent channels. The cycler can operate in two voltage operation ranges, namely: 0-5V and 0-20 V. The cycler can also operate in three different current ranges: 0-400 A, 0-40 A, and 0-5 A.

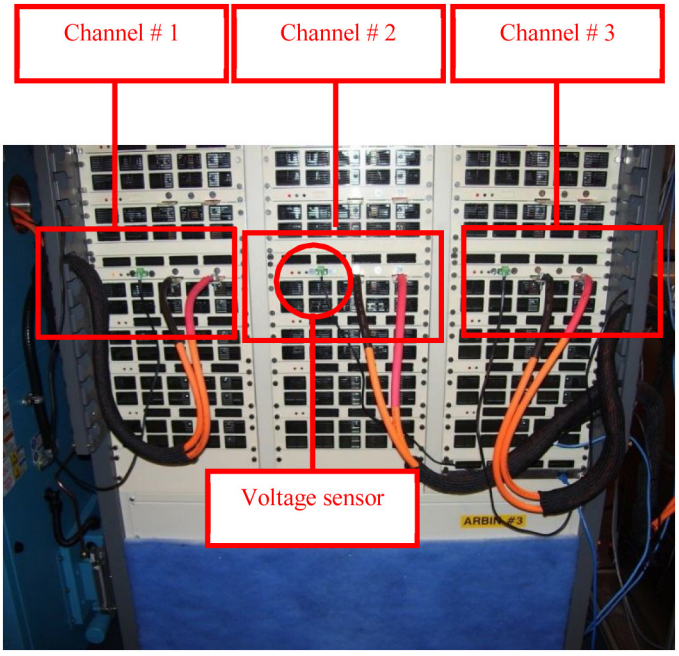

Figure 11. Arbin Cycler channels: channels equipped with voltage sensor and status indicator light.

PARAMETER IDENTIFICATION

An automated parameter estimation procedure [9] tracked the change in equivalent circuit parameters throughout the aging process. In addition, the method proposed in [10] increased the robustness of the estimation. The same approach was applied to each set of characterization data at 0, 15, 30, and 45 weeks of cycling. This estimation process is explained in detail in the following sections.

Equivalent Circuit Topology

An important part of the modeling process is choosing the equivalent circuit topology. The number of R-C pairs used in the equivalent circuit determines the capability of the model to match the measured transient responses. We performed an analysis on all of the relaxation events to determine the best accuracy we could achieve for the different number of R-C pair topologies.

Analyzing the Complexity and Accuracy Tradeoffs

Automating the process of curve fitting exponential decay equations to each relaxation period allowed for an efficient analysis of the cell dynamics. This analysis involved trying fittings using 1 to 5 exponential time constants (TC), each associated with R-C pairs in the circuit. A sample result at beginning of life is shown in Figure 12.

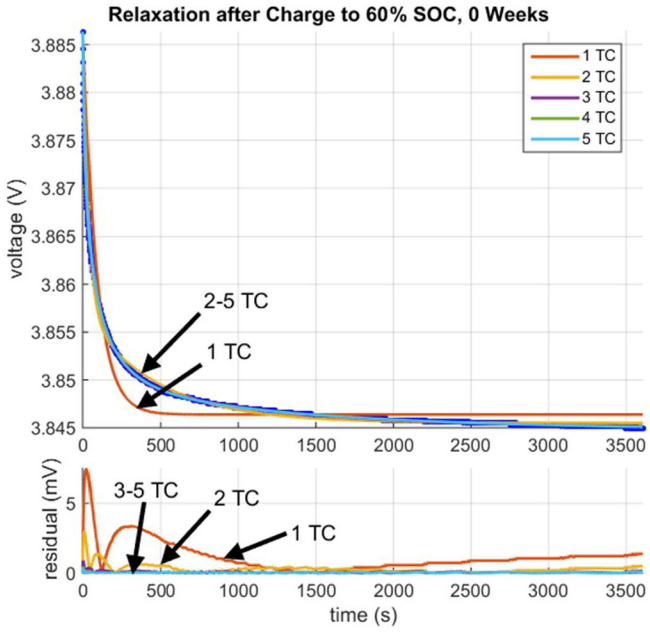

Figure 12. Relaxation curve fit.

By inspection, it was clear that the case of one time constant was much worse than all other options. Figure 13, Figure 14, and Figure 15 show a close-up of these results for one minute after a charge pulse that raised SOC from 55% to 60% at different stages of aging.

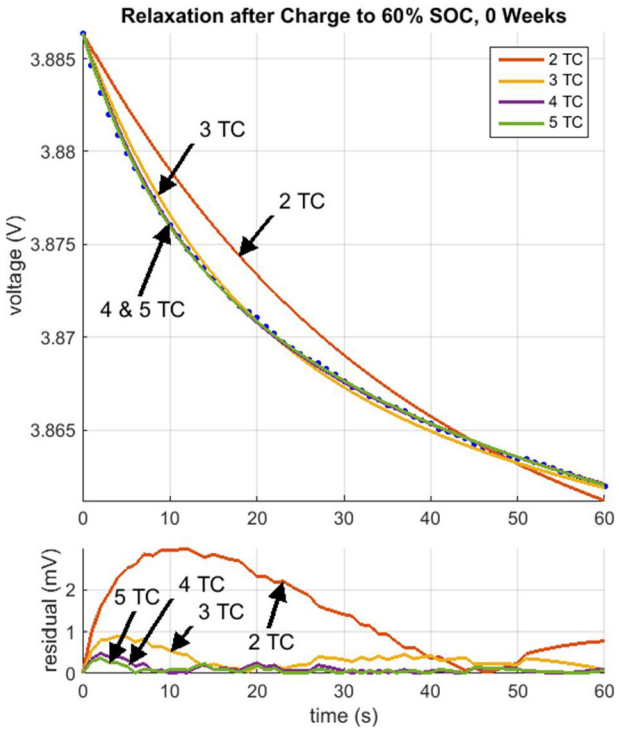

Figure 13. Relaxation curve fit at beginning of life.

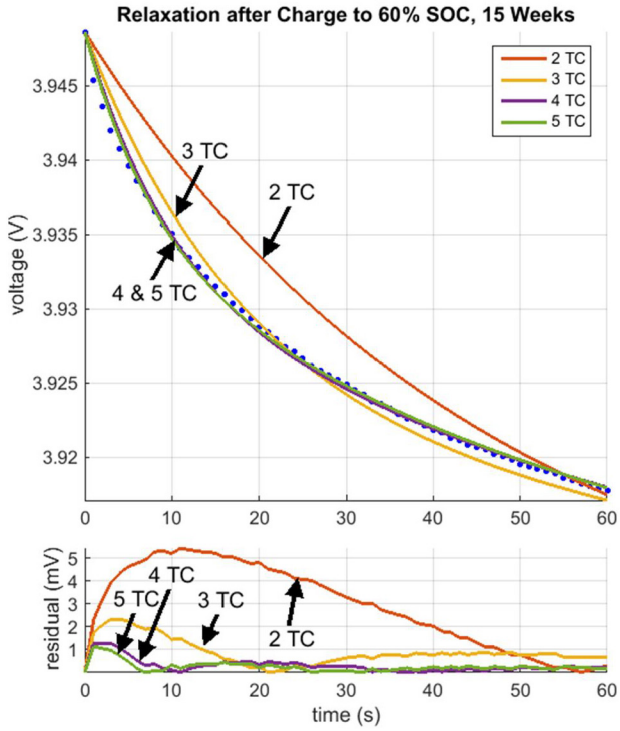

Figure 14. Relaxation curve fit at middle of life (15 weeks).

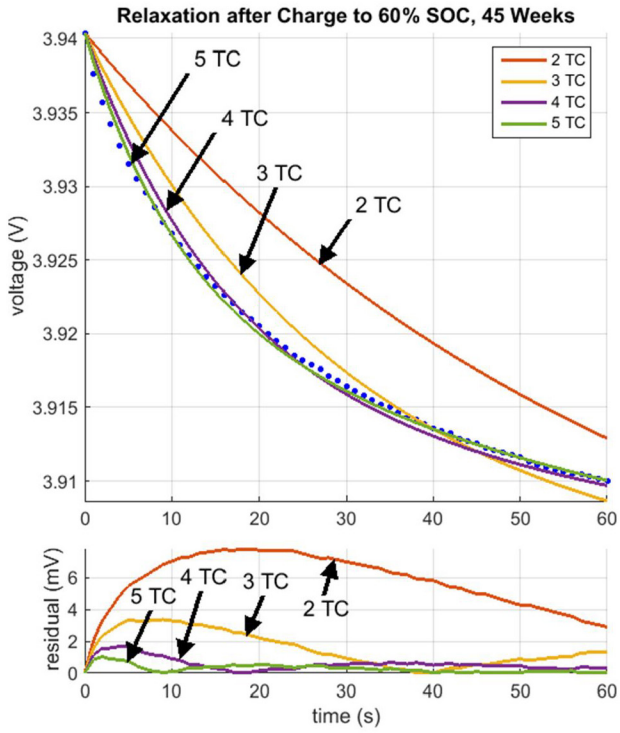

Figure 15. Relaxation curve fit at end of life (45 weeks).

Two conclusions arose from these results. First, we decided that three time constants was the minimum needed to achieve reasonable accuracy for the aging study. Second, we found that a more complex model structure was required to achieve equivalent accuracy at end-of-life due to additional physical processes as a result of the

aging process. For example, to keep the maximum voltage residual in the curve fit approximately 1 mV, we needed a 3 TC at beginning of life and a 5 TC by end of life.

Figure 16 shows a schematic of the 3 TC equivalent circuit used at beginning of life stages.

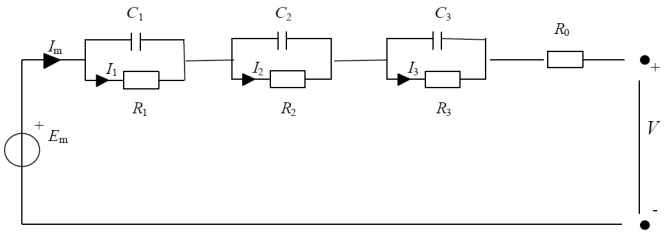

Figure 16. Equivalent circuit model with 3 R-C branches.

We used custom Simscape blocks for each element based on the technique described in [11]. Each of the circuit elements required a lookup table with SOC, SOH, temperature, and current as inputs. On the other hand, at the parameter estimation stage, each dataset varied only the SOC, keeping temperature, current, and SOH constants, so we used single input lookup tables in the model used for estimation purposes, as shown in Figure 17.

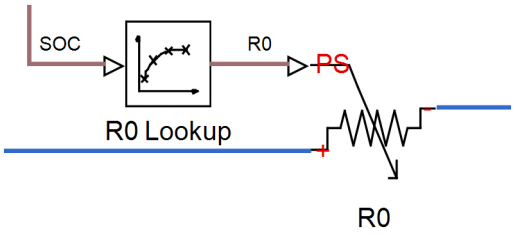

Figure 17. Single input lookup table for resistance.

Pulse Characterization Data

The pulse characterization data included a sequence of charge or discharge pulses, followed by a relaxation period, as shown in Figure 18.

The tests exercised the cells over their full SOC range, observing at the same time the manufacturer's specified voltage limits. The pulse widths were set to charge or discharge approximately 2% or 5% of the cell's rated capacity. At high and low SOC range, we used 2% pulse widths to better capture the abrupt changes in circuit parameters. In the mid-SOC range, we used 5% pulse widths to balance testing time versus the number of SOC points, e.g., resolution, on the parameter curves we would later obtain.

These tests allowed the transient dynamics of the R-C equivalent circuit to be isolated and observed at different SOC values. The pulse sequence was performed at a single operating point regarding the temperature, current, and SOH conditions. Figure 19 shows a simple example of how the elements of a 1 TC equivalent circuit affect the voltage response.

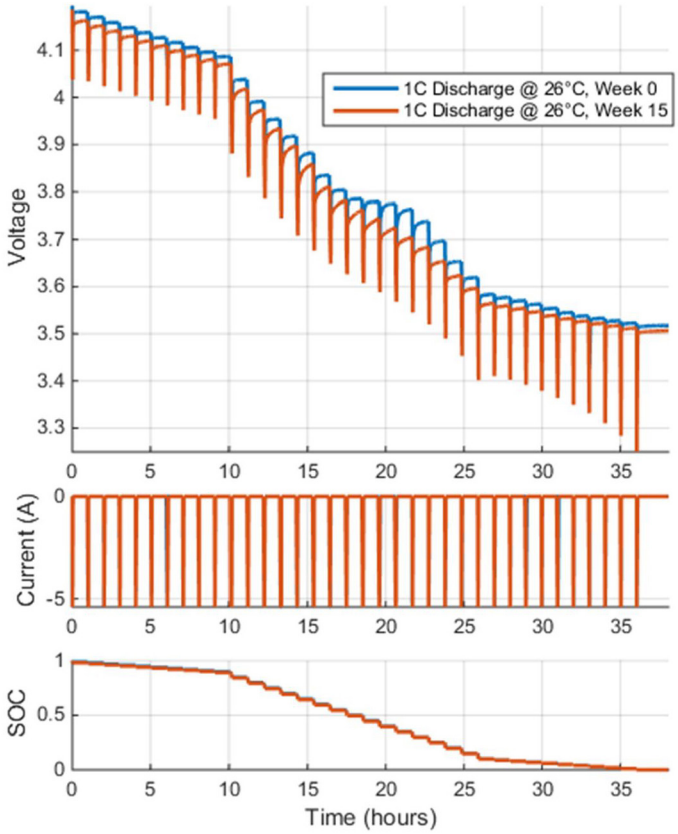

Figure 18. Pulse discharge characterization data.

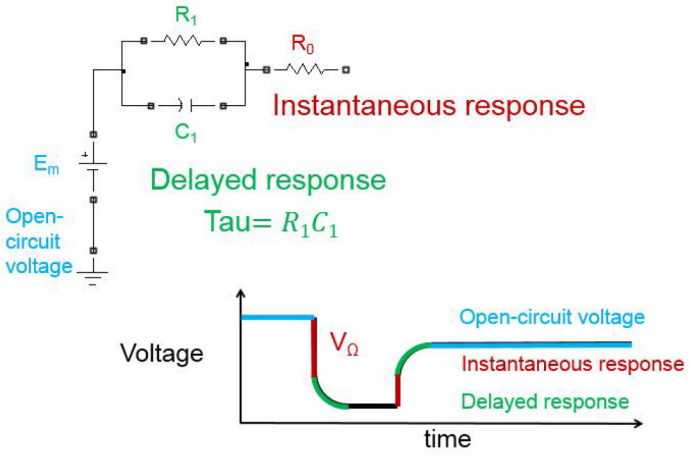

Figure 19. Schematic illustration of the relationship between observed voltage dynamics and a model equivalent circuit to reproduce those dynamics.

Automating the Parameter Estimation

Identification of Pulse and Relaxation Events

To perform parameter estimation, the first step is to automatically identify the pulse and relaxation events in the experimental data. Our MATLAB code observed the measured current for the pulse sequence characterization data and located the exact transition points. Our algorithm used this feature to characterize the portions of the data as a pulse event or a relaxation. The identification points for a single pulse are shown in Figure 20.

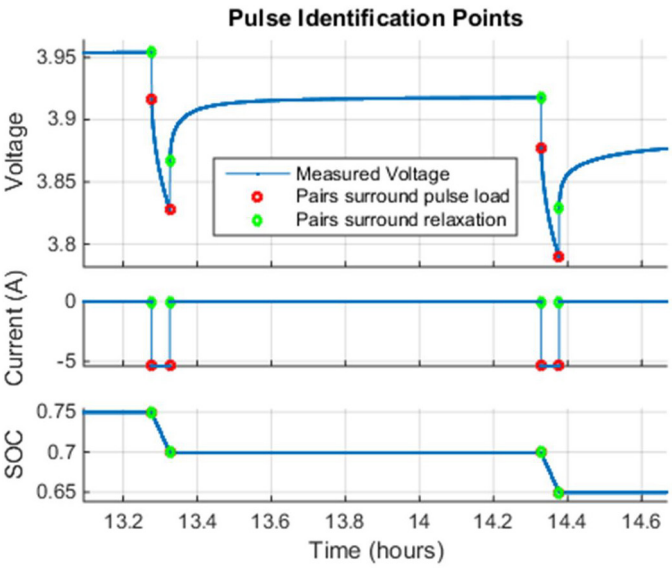

Figure 20. Automated identification results for the pulse and relaxation events.

Calculation of Initial Values

Open-Circuit Voltage and Series Resistance

In this step, we obtained initial guesses for the open-circuit voltage (OCV) and series resistance. These values correspond to the equivalent circuit elements E_m and R_0 from Figure 16. Our analysis was based on the voltages and currents at each transition between pulse events and relaxation.

To find the initial estimates for E_m, we assumed any transients had settled by the end of the relaxation period. The cell's terminal voltage would be approaching the OCV at the given SOC. This gave us a first approximation that could be further adjusted in a later step. Figure 21 shows an illustration of the data points we used to make these calculations for E_m and R_0 for the SOC 0.9 breakpoint.

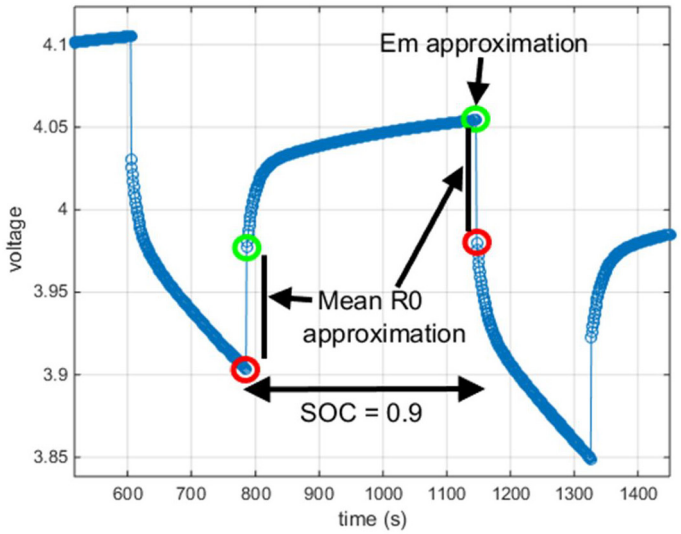

Figure 21. Approximating E_m and R_0.

It is important to note that the R_0 resistance values we calculated were affected by the choice of sample rate in the experimental data. Any portion of the transient dynamics that occurred in the finite time between data samples reflect the effective instantaneous voltage change at the transition point. Therefore, any dynamics that settled more quickly than we could measure in the sample rate were included in the initial estimate for resistance R_0.

An example of the initial results at this point is shown in Figure 22.

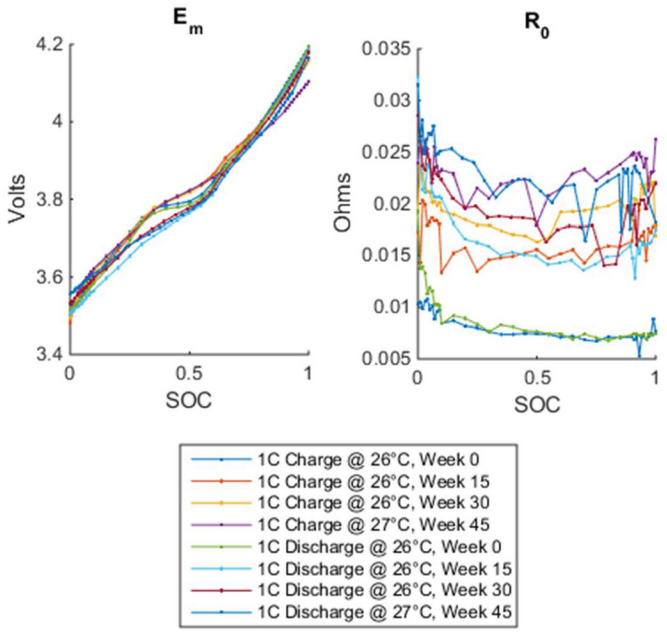

Figure 22. Initial estimates of E_m and R_0 versus SOC.

Relaxation Time Constants

Next, we identified initial values for the time constants during each relaxation phase in the experimental data. Subtracting out the open-circuit voltage, the relaxation dynamics observed at the terminals were governed solely by the initial voltages and time constants. For 3 R-C pairs, the voltage results:

$$V(t) = V_{ini} + \tau_1 \frac{dV_{C1}}{dt} + \tau_2 \frac{dV_{C2}}{dt} + \tau_3 \frac{dV_{C3}}{dt} - V_{C1_{ini}} - V_{C2_{ini}} - V_{C3_{ini}} \quad (1)$$

where V(t) was terminal voltage over time, V_{ini} was initial relaxation voltage, V_{Cn} were capacitor voltages, and $V_{Cn\ ini}$ were capacitor initial voltages beginning the relaxation.

A simple curve-fitting algorithm using the *fit* command in Curve Fitting Toolbox was implemented to determine initial values of the time constants. We used a *fittype* object with the standardized exponential expression of the form:

$$a_1 e^{-t/a_2} + b_1 e^{-t/b_2} + c_1 e^{-t/c_2} + V_{ini} - a_1 - b_1 - c_1 \quad (2)$$

where a_1, b_1, c_1 were initial capacitor voltages, a_2, b_2, c_2 were time constants, t was time, and V_{ini} was voltage at the start of relaxation. shows an example curve fit for one relaxation result.

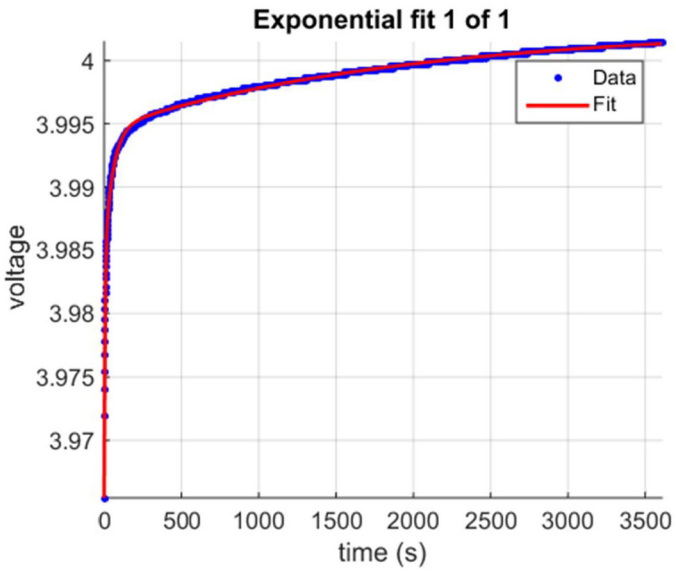

Figure 23. Relaxation curve fit to obtain initial time constant estimates.

Because there are many of these curve fits to process on several datasets and they are mutually independent, we ran these calculations concurrently using Parallel Computing Toolbox on an 8-core computer. Figure 24 shows the results for the three time constants.

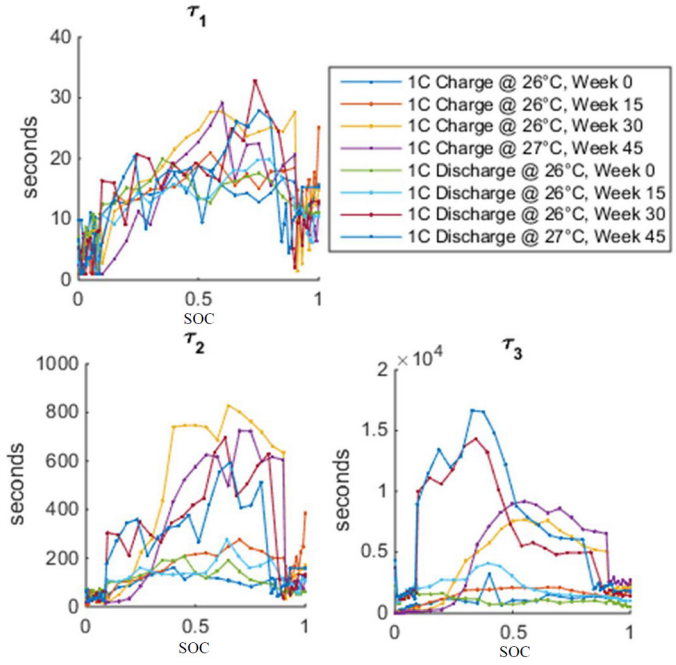

Figure 24. Initial time constant estimates from the curve fitting.

R-C Pair Resistances

To determine initial values of the resistances R_n where $n \geq 1$, we considered the transient dynamics. These resistances affected the voltage drop during load to the R-C pairs, but during relaxation it was not possible to isolate the resistance values from the R-C time constants. If we looked at one pulse event, the voltage response was driven by the series resistance and the R-C components:

$$V(t) = I(t) * R_0 + \tau_1 \frac{dV_{C1}}{dt} + \tau_2 \frac{dV_{C2}}{dt} + \tau_3 \frac{dV_{C3}}{dt} \quad (3)$$

This type of problem was analyzed numerically by treating the time-based experimental data as part of a linear system of equations to solve for the terminal voltage. However, we also considered that the resistance and capacitance values were changing during the pulse due to changes in SOC.

To find initial parameter values, we made the assumption that current was constant during the pulses. This allowed us to linearly scale the contributions of the parameter values from the starting SOC to the ending SOC during each pulse. The linear problem statement we posed was a matrix equation:

$$V(t) = V_{E_m} + V_{R_0} + V_{RC_1} + V_{RC_2} + V_{RC_3} \quad (4)$$

where the voltage contributions from each circuit element or R-C pair constituted the overall terminal voltage. The matrices' vertical dimension was time, and the horizontal dimension was SOC. The contribution of any given parameter showed up in the matrix only where it was relevant to the given SOC region in the experimental data. The linear system optimization problem was set up with the matrix equation:

$$v(t) = C(t) \cdot x \quad (5)$$

where v is a column of terminal voltage values versus time, x is a column-based parameter vector to be computed, and C is a matrix that provides the fractional contribution of every lookup table parameter (all SOC breakpoints) at every time sample. Example portions of the v(t) and C(t) matrices are shown in Figure 25.

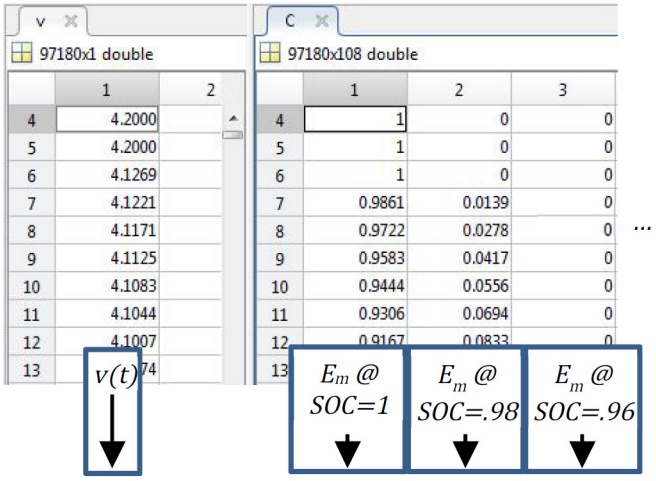

Figure 25. Linear system matrices example.

The parameter vector x was a long column matrix in the form:

$$\begin{bmatrix} E_{m\,@SOC=1} \\ E_{m\,@SOC=0.98} \\ \vdots \\ E_{m\,@SOC=0} \\ R_{0\,@SOC=1} \\ R_{0\,@SOC=0.98} \\ \vdots \\ R_{1\,@SOC=1} \\ \vdots \\ R_{2\,@SOC=1} \\ \vdots \end{bmatrix} \tag{6}$$

The least-squares optimization function LSQLIN in Optimization Toolbox was used to calculate the optimum parameter vector to minimize the matrix equation, using the objective:

$$\min_x \frac{1}{2}\|C \cdot x - v\|_2^2 \tag{7}$$

This produced a set of parameter values for the resistances R_n where $n \geq 1$. These values are shown in Figure 26.

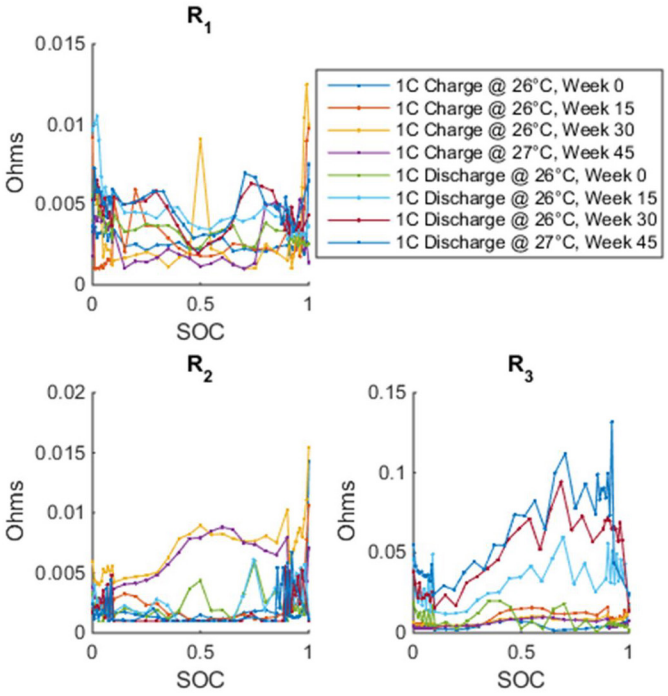

Figure 26. Initial resistance estimates from the linear optimization.

At this point, we have good initial estimates for the model parameters. If we simulate the entire pulse sequence at this point, we typically have a reasonable fit to the experimental data already, just based on the initial guesses. This is shown in Figure 27. This facilitates the next step of estimating the optimum overall parameter values.

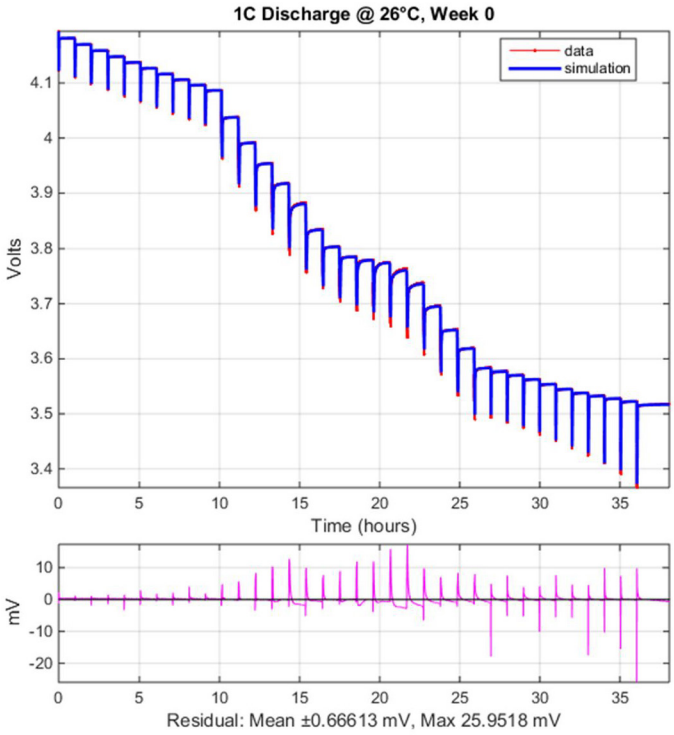

Figure 27. Experimental data and simulation results for one data set with initial parameter values, prior to final estimation process.

Parameter Estimation

The top level of the model was configured with current as the input signal with voltage and SOC outputs, as shown in Figure 28. This allowed us to connect the model to Simulink Design Optimization, so that we could estimate the final model parameters using our characterization data.

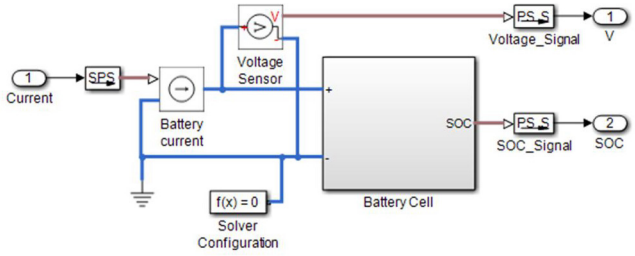

Figure 28. Top-level Simulink model.

We used Simulink Design Optimization to automatically loop through each pulse event, and estimate the optimum parameter values to match the measured data. This involved several setup steps:

1. Obtaining the transient data for each task
2. Assigning the transient data from a pulse to an experiment object associated with the model
3. Setting up each tunable parameter, including initial guess and valid range
4. Setting up estimation settings and parallel (multicore) estimation capabilities
5. Running the estimation task and gathering results

The breakdown of the data into estimation tasks was done using a layered approach [10]. For example, the first two tasks followed the format shown in Figure 29.

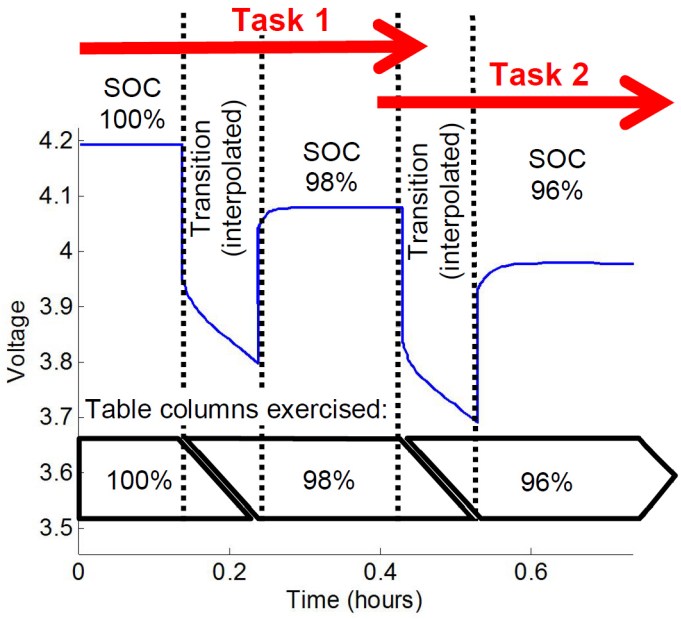

Figure 29. Illustration of the automated estimation process that layers estimation tasks in a pulse-by-pulse technique.

After each task, we also simulated the result to calculate the voltages across each R-C pair at the sample where the next task would begin. This was important in cases where the voltage did not fully settle during relaxation before the next pulse began. The simulated voltages were passed on to the estimation task to use as initial conditions.

The results for one estimation task are shown in Figure 30.

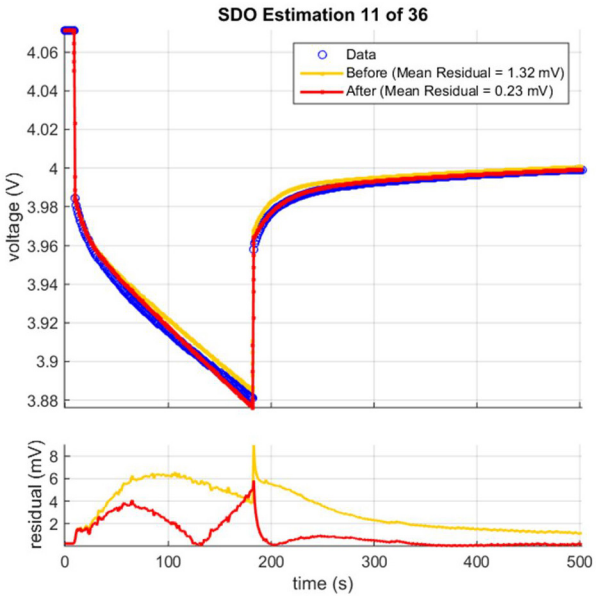

Figure 30. Result of one estimation task in the automated process.

After we completed all estimation tasks for a pulse sequence, we simulated the Simscape model using the complete pulse sequence current to compare the resulting voltage to the experimental data. One example result is shown in Figure 31.

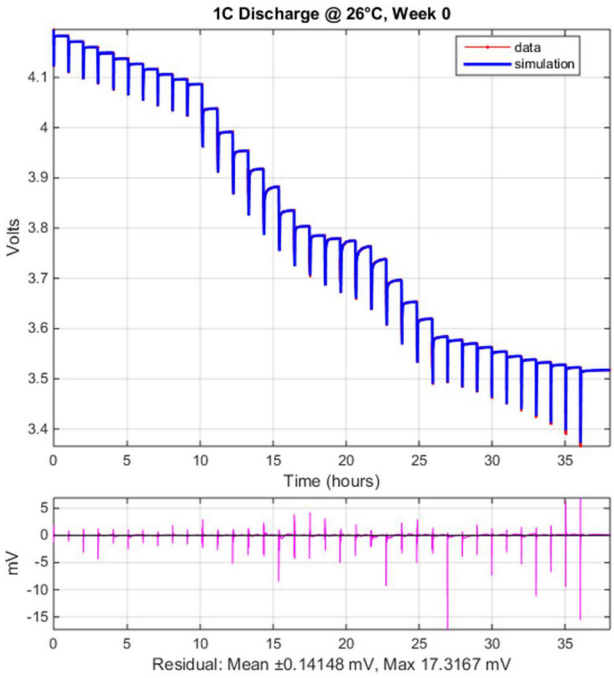

Figure 31. Experimental data and simulation results for one data set with initial parameter values, after final estimation process.

RESULTS

Lookup Tables

The output of this process was a set of lookup tables for the equivalent circuit parameters. For the single temperature and C-rate that we used, we found significant changes to the parameters. These tables are shown in Figure 32 (discharge) and Figure 33 (charge).

Observations

Figure 32 and Figure 33 show that the battery cell's properties changed significantly due to the aging experienced in our experiments. Two changes appear as dominant in terms of the aging effect on equivalent circuit parameters: internal resistance increase, leading to reduced power output capabilities; and recovery time increase, likely the result of impaired diffusion due to the appearance of new solid phases within the structure of electrodes and electrolyte.

The series resistance R_0 would likely have the greatest effect on the capabilities and application of the cell. Even after the first third of our aging experiment (15 weeks), the R_0 resistance had approximately doubled from its original value, thus reducing the power capability to half of the original value. By 45 weeks of aging, the resistance was about triple the initial value. This effect was consistent across the full SOC range.

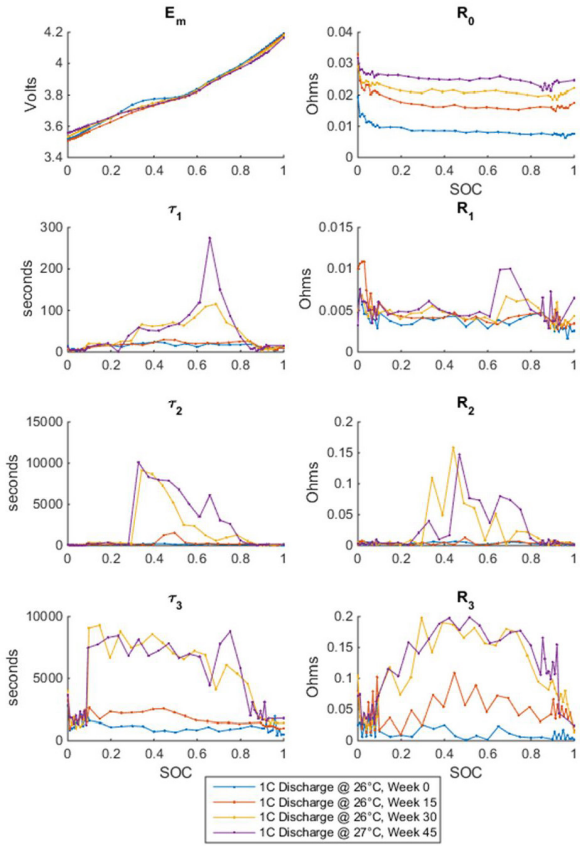

Figure 32. The optimized lookup tables for the 3 R-C equivalent circuit for different ages at 1C discharge rate.

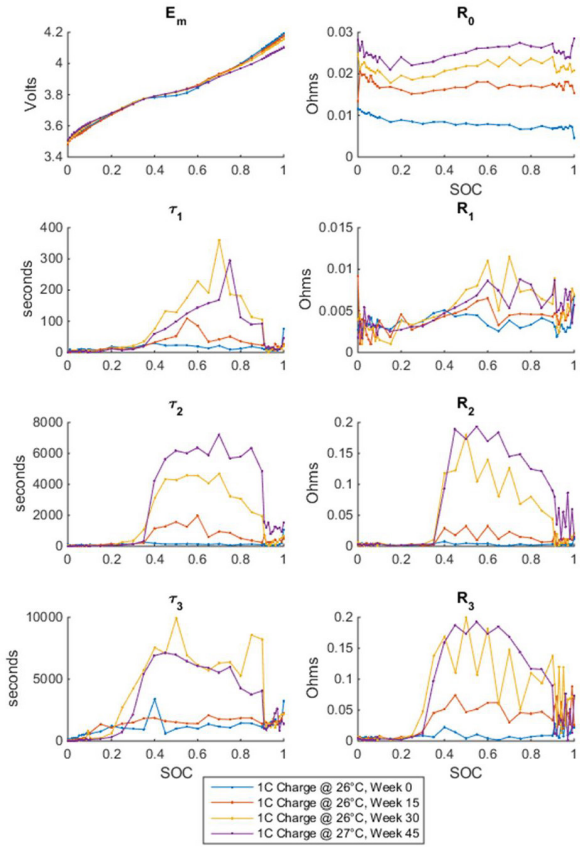

Figure 33. The optimized lookup tables for the 3 R-C equivalent circuit for different ages at 1C charge rate.

Model Validation

To assess the efficacy of the automated fitting process, model validation was performed using a subset of the Aging Schedule B drive cycle data for comparison. These drive cycles were used during the aging process of the battery, but were not directly used for parameter identification. Simulations, using the fit parameters, were compared with experimental battery voltage measurements from drive cycles. These drive cycles consist of both long-pulsed charge and discharge events, as well as rapid discharge cycles.

To validate the equivalent circuit battery model, the output terminal voltage of the model was compared to the measured experimental terminal voltage for identical battery current loads. The current load applied to both the experimental battery and the simulation is shown in Figure 34. The initial SOC conditions and static capacity of the experimental battery were used to initialize the simulation model. For each validation text, the experimental battery and the simulation began at an SOC of 86.6%.

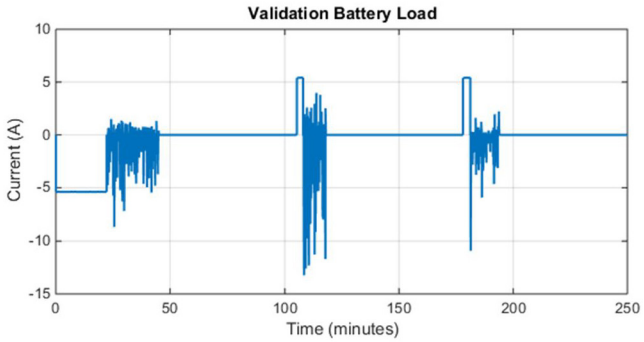

Figure 34. Drive cycle current load used for validation studies.

A comparison of the battery terminal voltages for both the experimental data and the simulation output can be seen in Figure 35 after 45 weeks of aging. As the pulse charge and discharge tests were conducted only with magnitude pulses of 5A, the parameters in the Simulink simulation are selected from a discharging or a charging lookup table according to the imposed current load. Figure 36 contains a detailed view of transient battery loading where the voltage residual increases as a result of fast dynamics.

Preliminary analysis of a unified lookup table for both charging discharging with interpolation between ±5A was found to not adequately represent the relaxation voltage recovery with 0A on the battery. The parameter characterization experiments used only pure discharge or charge scenarios, likely leading to polarization of active species in the battery cell. As such, the fit parameters represent only either charge relaxation or discharge relaxation and do not incorporate polarization hysteresis effects. For these validation studies, voltage relaxation was assumed to use the discharge parameters unless the battery was immediately subjected to a positive current.

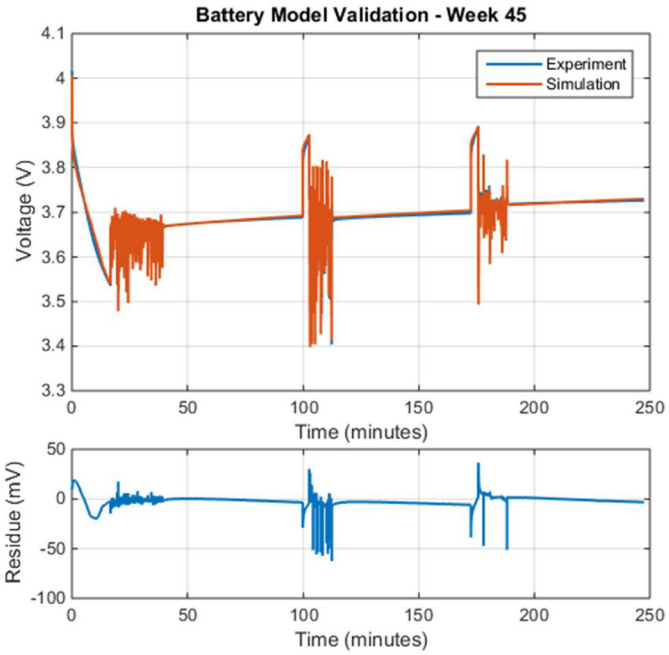

Figure 35. Simulation and experimental battery voltage comparison after 45 weeks of drive cycle aging.

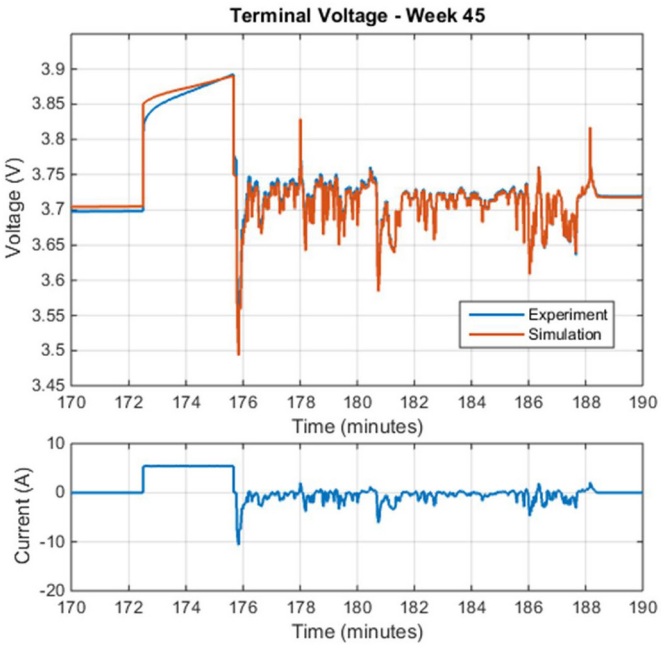

Figure 36. Subset of the validation study at 45 weeks of aging to highlight transients.

The validation study was performed for battery aging times of 0, 15, 30, and 45 weeks. The mean and maximum residuals for each validation test are summarized in Table 3.

Table 3. Mean and maximum residuals for validation studies at stages of battery degradation.

Battery Age (Weeks)	Mean Residual (mV)	Peak Residual (mV)
0	3.317	39.92
15	16.997	58.11
30	14.876	80.90
45	3.319	62.44

SUMMARY AND CONCLUSIONS

An automated, multistage parameter identification technique applied at different aging stages of a Li ion battery enabled the determination of changes in the cell parameters. An accelerated aging test used real-world driving cycles to degrade battery cell in terms of its internal resistance, capacity, and response time. Pulsed tests performed at 0, 15, 30, and 45 simulated weeks of cycling, showed significant changes in the cell behavior as a result of the cycling.

An equivalent circuit-based model with one voltage source, one series resistance, and several R-C pairs modeled the battery charge and discharge dynamics. Our results indicate that aging effects demand changes in the equivalent circuit topology. At beginning of life, three time constants were found to be sufficient to reproduce cell dynamics. However, at the battery end-of-life, a more complex model structure with five R-C pairs was required to achieve comparable accuracy.

Future research will involve testing the strategy at various operating temperatures and verifying the technique for battery packs.

REFERENCES

1. Andrea D., “Battery Management Systems for Large Lithium-Ion Battery Packs”, Norwood: Artech House, 2010.
2. Plett G. L., “Extended Kalman filtering for battery management systems of LiPB-based HEV battery packs: Part 3. State and parameter estimation,” Journal of Power Sources, no. 134, p. 277-292, 2004.
3. Plett G. L., “Extended Kalman filtering for battery management systems of LiPB-based HEV battery packs Part 2. Modeling and identification,” vol. 134, 2004.
4. Todeschini F., Onori S., and Rizzoni G., “An experimentally validated capacity degradation model for Li-Ion batteries in PHEVs applications,” Fault Detection, Supervision and Safety of Technical Processes, Volume # 8 | Part# 1, 2012.
5. Miller S., “Hybrid-Electric Vehicle Model in Simulink” http://www.mathworks.com/matlabcentral/fileexchange/28441-hybrid-electric-vehicle-model-in-simulink 10 Aug 2010. (Updated 17 Apr 2014) [Online].
6. “www.epa.gov/nvfel/testing/dynamometer.htm,” EPA United States Environmental Protection Agency. [Online].
7. “Battery Test Manual for Plug-In Hybrid Electric Vehicles,” U.S. Department of Energy, Idaho National Laboratory, Idaho Falls, Idaho 83415, March 2008.
8. “Plug-In Hybrid Electric Vehicle Value Proposition Study,” U.S. Department of Energy, ORNL/TM-2010/46, July, 2010.
9. Jackey R., da Cunha A. and Gazzarri J., “Webinar: Automating Battery Model Parameter Estimation using Experimental Data,” [Online]. Available: http://www.mathworks.com/videos/automating-battery-modelparameter-estimation-using-experimental-data-81987.html.

10. Jackey, R., Saginaw, M., Sanghvi, P., Gazzarri, J. et al., "Battery Model Parameter Estimation Using a Layered Technique: An Example Using a Lithium Iron Phosphate Cell," SAE Technical Paper 2013-01-1547, 2013, doi:10.4271/2013-01-1547.
11. Huria T., Ceraolo M., Gazzarri J., and Jackey R., "High fidelity electrical model with thermal dependence for characterization and simulation of high power lithium battery cells," Electric Vehicle Conference (IEVC), March 2012.

ABBREVIATIONS/DEFINITIONS

BEV - Battery Electric Vehicle

BMS - Battery Management System

CCCV - Constant Current Constant Voltage, a method for charging Li-Ion batteries.

E_m - voltage source of an equivalent circuit model that represents the open circuit voltage

EV - Electric Vehicle

HEV - Hybrid Electric Vehicle

HPPC - high-performance pulse characterization data, a type of experimental data which contains discharge and pulse discharges at different SOC values

HWFET - The Highway Fuel Economy Driving Schedule represents highway driving conditions under 60 mph.

LiNiMnCoO2 - Lithium Nickel-Manganese-Cobalt Oxide, a type of battery cell

NMC - lithium nickel-manganese-cobalt oxide, a type of battery cell

OCV - open circuit voltage (V)

PHEV - Plug-in Hybrid Electric Vehicle

R_n - variable resistor n of an equivalent circuit model

R-C branch - a portion of an equivalent circuit comprised of a parallel variable resistor and variable capacitor

SOC - State Of Charge as a fraction of the total cell capacity, ranging from 0 to 1 (or 0% to 100%)

SOH - State Of Health, an arbitrary number normally defined as 100% meaning the battery meets its specifications and 0% meaning the battery is completely depleted. []

SOP - State Of Power is the capability of the battery to charge / discharge at a specific level.

τ_n - time constant n for an R-C branch of an equivalent circuit model

UDDS - The EPA Urban Dynamometer Driving Schedule, commonly called the "LA4" or "the city test" and represents city driving conditions.

US06 - The US06 is a high acceleration aggressive driving schedule that is often identified as the "Supplemental FTP" driving schedule.